Journal of Materials Chemistry A

PAPER

View Article Online
View Journal | View Issue

Cite this: J. Mater. Chem. A, 2018, 6, 21567

Mussel-inspired polydopamine chemistry to modulate template synthesis of 1D metal–organic framework superstructures†

Boxuan Yu,[ac] Gang Ye,*[ab] Zhen Zeng,[a] Lei Zhang,[a] Jing Chen*[ab] and Shengqian Ma*[c]

Received 1st September 2018
Accepted 19th October 2018

DOI: 10.1039/c8ta08514e

rsc.li/materials-a

Mussel-inspired polydopamine (PDA) chemistry was exploited, for the first time, to regulate the contra-diffusion synthesis of 1D metal–organic framework (MOF) superstructures in the channels of polycarbonate track-etched membranes. The PDA modified template channels facilitate controllability for the heterogeneous nucleation and interfacial growth of various MOFs. Well-defined 1D hybrid MOF nanotubes with a high aspect ratio up to 40 and length of 10 μm were successfully obtained. Potential application of the composite membrane for decontamination of organic dyes was demonstrated by a facile filtration method. This study provides new insights into the surface chemistry directed growth behavior of MOFs on polymeric templates. Moreover, the methodology of PDA chemistry mediated contra-diffusion synthesis opens a new avenue to fabricate diverse 1D superstructures of MOFs and other functional materials.

Introduction

Metal–organic frameworks (MOFs) are a class of fascinating crystalline hybrid materials with ordered three-dimensional structures constructed through the formation of coordination bonds between metal ions/clusters as nodes and organic ligands as linkers.[1–3] Open framework structures and diverse functional groups in ligands, such as amino and carbonyl, offer large specific surface area and task-specific designability,[4–6] making MOFs emerge as a type of porous material with significant prospects for application in many fields, including gas adsorption,[7–10] catalysis,[11–13] environmental remediation,[14–17] *etc.*[18–21]

While substantial efforts have been devoted to the synthesis of new MOFs and the exploration of their new applications in the past decade, developing synthetic strategies for controllable fabrication of zero-, one-, two-, or three-dimensional MOF architectures is a burgeoning area attracting escalating attention.[22–26] In particular, assembling MOF crystals into one-dimensional (1D) superstructures not only provides a bridge between the nanoscale regime and meso- or macroscale objects, but also holds great potential for applications in gas adsorption,[27] sensing,[28] and optoelectronics.[29] Although composite 1D porous superstructures supported by specific organic or inorganic substrates have been reported previously,[30–32] self-supported 1D superstructures,[33–35] especially those with tailor-made hollow structures, have rarely been achieved.

Among the methodologies for building 1D MOF superstructures, macro-structural template (hard template) synthesis represents one of the facile yet versatile synthetic approaches.[36,37] However, given that the formation of MOFs occurs in the reaction solution, very few crystals can be anchored to the surfaces and pore channels of native substrates, thereby failing to form well-defined 1D superstructures, especially for inert templates with complicated structural features.[38] To overcome this limitation, seed coating[28] or surface modification[39] is usually required to promote the heterogeneous nucleation of MOF crystals. In this regard, a dynamic step-by-step method on anodic aluminum oxide (AAO) was proposed to confine the nucleation and growth of MOF crystals within the template system.[40] However, due to the weak interaction between the inert surface of AAO and the MOF nucleus, the MOFs in the channels were prone to accumulation on both sides of AAO, blocking the porous channels and making it difficult to form continuous 1D MOF superstructures spanning across the whole channel.[41]

Mussel-inspired polydopamine (PDA) chemistry, since the pioneering work of Messersmith in 2007,[42] has received considerable attention as a versatile surface modification technique.[43–45] Taking advantage of the self-polymerization of dopamine under aerobic and alkaline conditions, the generated PDA nanoparticles can be homogeneously deposited to virtually any surface, forming a tightly adhesive layer.[46,47] Moreover, the

[a]Collaborative Innovation Center of Advanced Nuclear Energy Technology, Institute of Nuclear and New Energy Technology, Tsinghua University, Beijing, 100084, China. E-mail: yegang@mail.tsinghua.edu.cn; jingxia@mail.tsinghua.edu.cn

[b]Beijing Key Lab of Radioactive Waste Treatment, Tsinghua University, Beijing 100084, China

[c]Department of Chemistry, University of South Florida, 4202 E. Fowler Avenue, Tampa, FL 33620, USA. E-mail: sqma@usf.edu

† Electronic supplementary information (ESI) available. See DOI: 10.1039/c8ta08514e

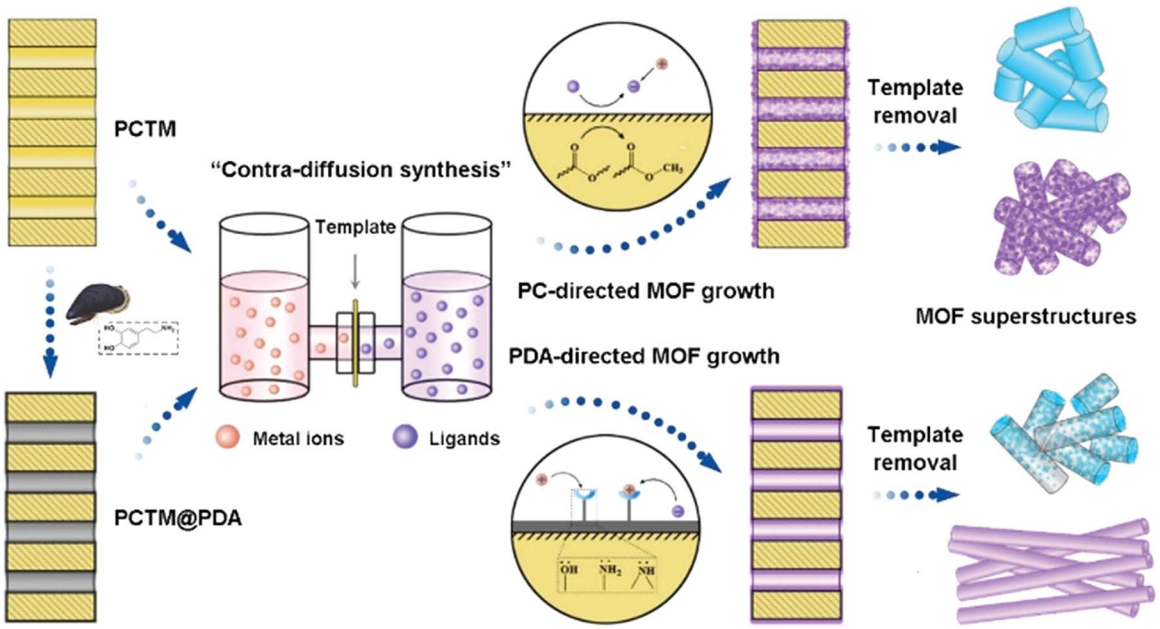

Scheme 1 Illustration of surface chemistry directed template synthesis of metal–organic framework (MOF) superstructures using a contra-diffusion method in pristine and polydopamine (PDA) modified polycarbonate track-etched membrane (PCTM) templates.

existence of abundant functional groups such as catechol and amine in PDA makes it an ideal platform to coordinate metal ions.[48–50] This can provide nucleation sites and anchor bars to accommodate MOF crystals on inert surfaces, facilitating the construction of 1D MOF architectures in diverse templates.

Herein, we report, for the first time, the PDA chemistry modulated controllable synthesis of 1D MOF superstructures using a facile contra-diffusion synthetic strategy (Scheme 1)[51–53] in the uniform cylindrical pores of polymeric membranes prepared by a track-etching technique.[54,55] It is highlighted that the heterogeneous nucleation and growth behaviors of MOF crystals can be tuned by altering the surface chemistry of the pore channels. Within the pore channels of the native polycarbonate (PC) membrane, a catalytic transesterification mechanism was revealed which led to the activation of imidazole ligands to promote the nucleation of ZIF-8 crystals.[56–58] In particular, taking advantage of the bio-inspired PDA chemistry, surface engineering of the pore channels was achieved, which greatly improved the controllability of the template synthesis of 1D MOF superstructures with enhanced structural stability, facilitating the formation of well-defined 1D ZIF-8 nanotubes spanning across the template channels with an aspect ratio up to 40. This strategy can be readily extended to the synthesis of other 1D MOF superstructures, such as ZIF-67, ZIF-12, and HKUST-1. Moreover, the obtained ZIF-8 composite membrane could efficiently separate organic dye contaminants in a simple flow-through mode.

Experimental

Materials

Sodium hydroxide (98%), zinc nitrate hexahydrate (99.5%), copper nitrate trihydrate (99.5%), cobalt nitrate (99%), ethyl acetate (99%, AR), and dichloromethane (99.5%, AR) were bought from Beijing Chemical Works. Dopamine hydrochloride (DA, 98%), methanol (99.9%, ACS/HPLC certified), ethanol (99.9%, ACS/HPLC certified), 1,3,5-benzenetricarboxylic acid (99%), 2-methylimidazole (99%), and benzimidazole (98%) were supplied by J&K Scientific Co., Ltd. Tris(hydroxymethyl)aminomethane (Tris) (>99%) and methylene blue (>95%) were purchased from Sigma-Aldrich. Deionized water was used for the preparation of all aqueous solutions. All reagents were used as received without further purification. Polycarbonate (PC) membrane was purchased from Bayer Company.

Preparation of PCTMs

The polycarbonate track-etched membranes (PCTMs) were prepared according to our previously reported method.[59,60] Firstly, PC membranes with a thickness of 10 μm were irradiated with Kr^{84} ions on a heavy ion accelerator at normal incidence. After exposure to ultraviolet (UV) light for 1 hour on each side, the sensitized membranes were fixed on a mould and immersed in 6.25 mol L^{-1} NaOH aqueous solution at 50 °C for 10 min. After chemical etching, the obtained PCTMs were rinsed three times with deionized water under ultrasonication and then dried at room temperature.

Modification of the PCTM *via* PDA deposition

A piece of the as-prepared PCTM was fixed on a mould and washed with deionized water, followed by immersion into 10 mM Tris–HCl (pH = 8.5) buffer. After vacuum treatment for 30 min to expel the air present in the pores, dopamine hydrochloride solution was added dropwise into the buffer under mechanical and magnetic stirring (200 rpm) on both sides of the PCTM (Fig. S1†). The total concentration of dopamine

hydrochloride in the buffer was 1 g L^{-1} and the deposition process lasted 8 hours at room temperature. Then, the PDA modified PCTM was rinsed in de-ionized water with ultrasonication, and then dried in a vacuum oven at 50 °C.

Contra-diffusion synthesis of MOFs within PCTM pore channels

A series of MOFs including ZIF-8, HKUST-1, ZIF-67, and ZIF-12 were synthesized within the pore channels of the PDA modified PCTM *via* a contra-diffusion method.[51–53] Taking the template synthesis of ZIF-8 as an example, zinc nitrate hexahydrate (297 mg, 1 mmol) and 2-methylimidazole (328 mg, 4 mmol) were dissolved in 20 mL methanol, respectively. A piece of PDA modified PCTM was then immersed in the zinc nitrate/methanol solution for 30 min following by slight dipping in methanol, enabling the pre-coordination of Zn^{2+} with the PDA coating. After that, the PCTM was mounted between the two chambers of a contra-diffusion cell, and zinc nitrate solution and 2-methylimidazole solution were synchronously added into different chambers. After one hour, the functionalized PCTM was dipped in methanol several times to wash off the loose crystals on the surface and dried under vacuum at 50 °C. The digital photo of the reaction setup is shown in Fig. S2.† For control experiments, a piece of pristine PCTM without PDA modification of the pore channels was employed for contra-diffusion synthesis of 1D MOFs according to the same recipe described above. For the synthesis of other MOFs, all the ZIFs were synthesized using the same molar concentration of precursor solution. But for HKUST-1, 1 mmol copper nitrate trihydrate (241 mg) and 1.33 mmol 1,3,5-benzenetricarboxylic acid (280 mg) were used to prepare the precursor solution. To obtain the 1D superstructure of the MOFs, the membrane templates were dissolved in dichloromethane. Self-supported 1D MOF superstructures were collected by centrifugation, followed by repeated washing in methanol and drying under vacuum at 50 °C.

Separation performance of organic dyes

The separation performance to remove methylene blue from aqueous solution was demonstrated in a filtration mode using the ZIF-8 functionalized PCTM. A piece of ZIF-8 functionalized PCTM was fixed in a membrane vacuum filtration apparatus. 3 mL methylene blue solution (5 mg L^{-1}) was introduced to the apparatus at room temperature. The solution passed through the functionalized PCTM assisted by a vacuum pump (vacuum degree $\sim$ 0.09 MPa) at a flow rate of $\sim$3 mL min^{-1}. The concentrations of the original methylene blue solution and the filtrates were also determined by UV-vis spectrometry.

Characterization

Scanning electron microscopy (SEM) was conducted by using a ZEISS MERLIN and FEI QUANTA 200 scanning electron microscope. The sample was disposed with metal or carbon spraying before observation. It was observed at an accelerating voltage of 30 kV under vacuum conditions after metal spraying. Transmission electron microscopy (TEM) images were recorded by using a model H-7700 microscope with an accelerating voltage of 120 kV. Fourier transform infrared (FT-IR) spectra were recorded on a Nicolet iN10 Infrared Microscope. Powder X-ray diffraction (XRD) patterns were obtained on a diffractometer with Cu Kα radiation, with a scan step of 0.2° and the scan range between 3° and 50°. Nitrogen adsorption–desorption isotherms were measured with a NOVA 3200e Surface Area & Pore Size Analyzer. Samples were dried at 80 °C (for PCTM) or 120 °C (for nanotubes) under vacuum for at least 3 h before the nitrogen adsorption experiments. Specific surface areas were calculated based upon the Brunauer–Emmett–Teller (BET) method. UV-vis spectra between 200 and 800 nm were recorded at room temperature with a Cary 6000i spectrometer using a 1 cm path length quartz cuvette. Thermogravimetric analysis (TGA) was conducted on a TA Instruments SDT Q600 with a heating rate of 10 °C min^{-1} from 30 °C to 900 °C. Samples weighing between 10 and 20 mg were heated in a N_2 flow (100 mL min^{-1}).

Results and discussion

To study the nucleation and growth behavior of MOF crystals within the confined microchannels of the polycarbonate track-etched membrane (PCTM), two classes of MOFs with different crystalline structures, *i.e.*, ZIF-8 and HKUST-1, were chosen as prototypes due to their structural stability and mild synthesis compatible with the polymeric templates. The former is made up of zinc ions coordinated by four imidazolate rings with a pore aperture of *ca.* 3.4 Å, while the latter, made up of copper paddlewheel nodes with 1,3,5-benzenetricarboxylate (BTC) struts, features three distinct internal pores (two of comparable size, *ca.* 14 Å, and a smaller pore *ca.* 10 Å) (Fig. S3†).[61] The surface and section morphologies of pristine PCTM observed under a SEM are shown in Fig. 1a and b. Cylindrical pore channels with a diameter of 260 nm were observed spanning across the whole thickness of the membrane. The inset in Fig. 1a shows the digital photo of a native PCTM.

In a contra-diffusion synthesis, a piece of PCTM was employed to separate the two chambers containing the solutions of metal ions and ligands (Fig. S2†). The concentration gradient driven diffusion across the PCTM resulted in the nucleation and growth of MOF crystals within the pore channels. The SEM section view in Fig. 1c shows that a large number of ZIF-8 crystals were formed inside the pore channels. After dissolving the template, well-defined hollow 1D ZIF-8 superstructures constructed from intergrown crystal nanoparticles were obtained (Fig. 1e). The 1D ZIF-8 superstructure replicated the dimensional features of the pore channels. XRD analysis confirmed the ZIF-8 structure generated in the PCTM template and isolated 1D superstructures, which was consistent with the conventional ZIF-8 crystals (Fig. S4†). Selected area electron diffraction analysis (Fig. 1e, inset) suggested the polycrystalline nature of the ZIF-8 superstructure. For the case of HKUST-1, however, only a few intergrown nanocrystals were found at the entrances of the pore channels (Fig. 1d). After template removal, solid HKUST-1 nanorods of less than 1 μm were obtained (Fig. 1f), suggesting a limited diffusion path of the ligands during the synthesis. This may be attributed to the relatively

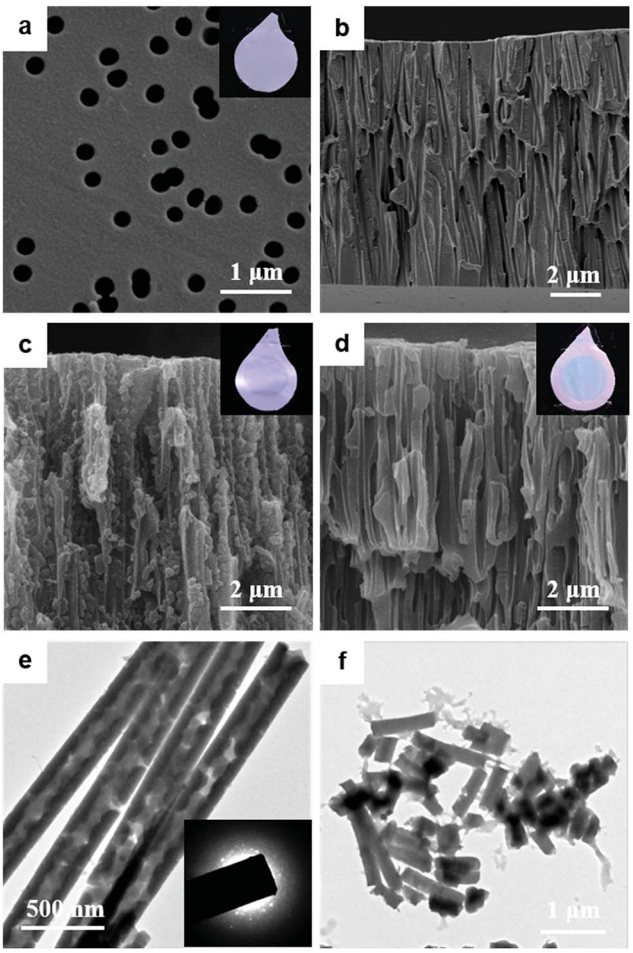

Fig. 1 Surface (a) and section view (b) SEM images of the pristine polycarbonate track-etched membrane; section view SEM images of PCTMs deposited by ZIF-8 (c) and HKUST-1 (d); TEM images of isolated ZIF-8 (e) and HKUST-1 (f) superstructures after membrane dissolution; the insets are the digital photos of the corresponding membranes and electron diffraction pattern of ZIF-8 nanotubes.

larger size of the HKUST-1 crystals under the experimental conditions (Fig. S5†), blocking the pore entrances and preventing further diffusion of the ligands.

Meanwhile, a more careful examination of the 1D ZIF-8 superstructures shows a continuous growth of the ZIF crystals along the pore walls with clearly resolved thick boundaries (Fig. 1e), which implies the potential influence of the surface chemistry of the polycarbonate templates on the nucleation and growth of the ZIF-8 crystals. It is known that imidazole compounds can catalyze transesterification reactions.[56–58] Hence we speculated that, for the template synthesis of ZIF-8 on PCTMs, the interaction between the imidazole ligands and the polycarbonate matrix might play an important role in the crystallization process of the ZIF-8 crystals. To verify this point, solvent synthesis of ZIF-8 with the introduction of ethyl acetate as a nucleation agent was performed. The digital photo in Fig. 2a records the synthesis of ZIF-8 catalyzed by different additions of ethyl acetate. Apparently, a higher dosage of ethyl acetate resulted in a faster crystallization rate of ZIF-8. Meanwhile, an evident decrease of the average particle size from 98 nm to 23 nm was observed under TEM (Fig. 2b–d), suggesting the promotion of nucleation rate with the aid of ethyl acetate.[62]

In a typical synthesis of ZIF-8, the formation of 2-methylimidazole (mIM) anions *via* deprotonation is basically a key step to promote the nucleation and growth of ZIF-8 crystals.[63] Upon contact with ester compounds, mIM ligands can catalyze a transesterification reaction according to an established mechanism shown in Fig. 3. The catalytic cycle results in the generation of deprotonated mIM ligands. This is expected to activate the coordination between the mIM ligands and the metal ions. Such an understanding helps to elucidate the nucleation and growth behavior of MOF crystals in the pore channels of PCTMs. For the template synthesis of ZIF-8, the mIM ligands diffuse into the pore channels and catalyze the transesterification reaction of polycarbonate, which generates a relatively high concentration of activated mIM ligands, thereby inducing the preferential nucleation and growth of ZIF-8 crystals adherent to the pore walls without blocking the channels. Therefore, after removing the template, hollow 1D ZIF-8 superstructures with thick boundaries were obtained. It is worth mentioning that the imidazole-catalyzed transesterification reaction can also be proven by the mechanical strength change of the polycarbonate membrane. After 3 h of contra-diffusion synthesis, the polycarbonate membrane exhibited a sharp decrease in the mechanical strength and a fragile composite membrane was finally obtained after 6 h (Fig. S6†). In contrast, due to the poor interaction between the BTC ligands and the polycarbonate matrix, the growth of

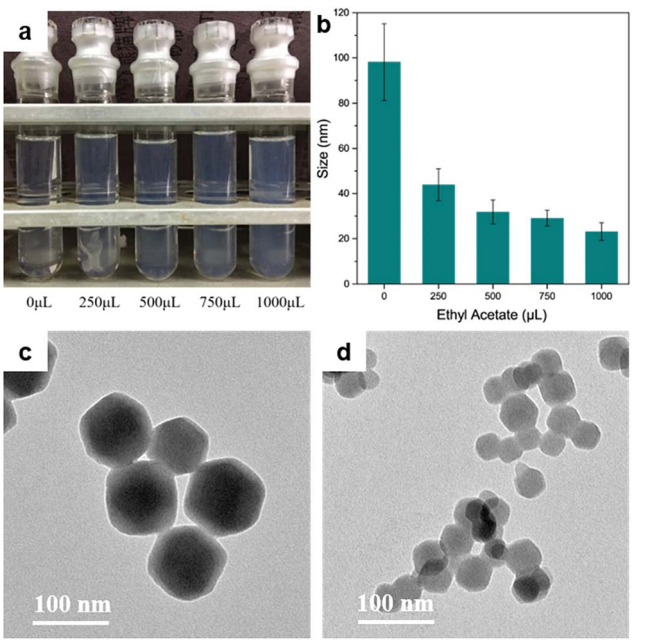

Fig. 2 (a) Photograph of ZIF-8 synthesis catalysed by different additions of ethyl acetate at 5 min; (b) average size of ZIF-8 particles synthesized in the presence of various concentrations of ethyl acetate after 1 h; TEM images of ZIF-8 crystals prepared (c) without catalyst and (d) with 500 μL ethyl acetate after 1 h.

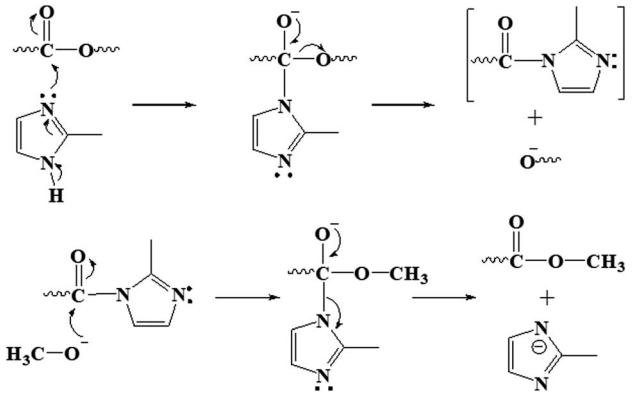

Fig. 3 Mechanism of transesterification reaction catalysed by 2-methylimidazole.

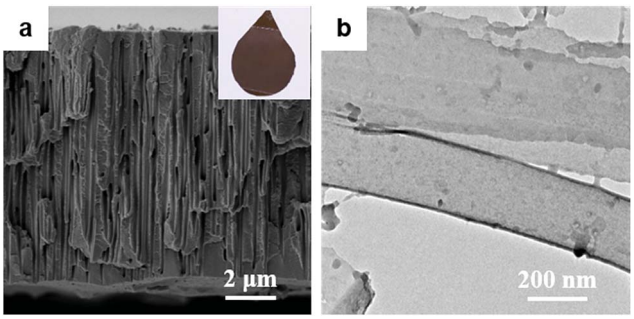

Fig. 4 (a) Section view SEM image of the PDA modified PCTM and (b) TEM image of a PDA nanotube after membrane dissolution. The inset shows the digital photo of a piece of PDA modified PCTM.

HKUST-1 crystals was not confined to the surfaces of the pore walls. The large-sized HKUST-1 crystals accumulated at the entrance of the pores, preventing the continuous diffusion of BTC ligands into the channels. Thus, only short HKUST-1 nanorods were obtained after removing the PCTM templates.

Although the surface directed growth of ZIF-8 realized the preparation of hollow 1D MOF superstructures, the relatively large crystal size with non-uniform stacking did not provide ideal channels with a homogeneous inner diameter. Due to the poor interfacial strength, cracks and fractures were often found for the isolated 1D ZIF-8 superstructures (Fig. S7†). Furthermore, as mentioned above, the sacrifice of membrane strength also hindered the fabrication of a robust composite membrane for separation applications. To address this challenge, mussel-inspired polydopamine (PDA) chemistry was exploited for surface engineering of the pore channels of PCTMs. It can be envisioned that the establishment of a PDA platform rich in catechol and amine groups on the pore surfaces would provide an ideal environment to accommodate metal ions, facilitating the heterogeneous nucleation and interfacial growth of MOF crystals.[64] Meanwhile, the PDA interface would enhance the mechanical strength of the composite membrane as well as isolated 1D MOF superstructures.

To facilitate the effective modification of the inner surfaces of the PCTM, the polymerization of dopamine was performed in a laboratory-made apparatus (Fig. S1†) with the membrane suspended in the reaction solution. Strong shear force was provided by rigorous stirring to prevent the blocking of the pore entrances by some of the large-sized PDA aggregates. Fig. 4a shows the section view SEM image of the PDA modified PCTM with well-preserved pore arrays. The color change of the membrane from white to dark brown (Fig. 4a, inset) indicates the deposition of PDA. Conformal PDA nanotubes with a wall thickness of *ca.* 12 nm were obtained after template dissolution, suggesting the generation of uniform PDA layers on the inner surfaces of the pore arrays (Fig. 4b). Further evidence to support the successful formation of the PDA layer was provided by ATR-FTIR analysis. The characteristic peak in the ATR-FTIR spectrum (Fig. 5a, blue) at 1601 cm^{-1} is assigned to the bending vibration of the aromatic ring which is absent in the spectrum of pristine PC membrane (Fig. 5a, black). Additionally, the broad peak spanning from 3600 cm^{-1} to 3000 cm^{-1} corresponds to the O–H and N–H stretching vibrations in the PDA structure.[65]

Then, ZIF-8 was employed as a prototype for fabricating 1D MOF superstructures from the PDA modified PCTM templates. After the contra-diffusion synthesis, the pore arrays of the membrane were retained (Fig. 6a) with small-sized ZIF-8 nanoparticles homogeneously deposited on the inner surfaces (Fig. S8†). Template removal resulted in well-defined 1D hollow ZIF-8 nanotubes replicating the dimensions of the pore arrays (Fig. 6b). The nanotubes showed greatly improved structural regularity compared to those obtained from native PCTM templates. Uniform channels with an inner diameter of 150 nm could be observed. Particularly, massive production of the 1D ZIF-8 nanotubes with identical length (*ca.* 10 μm) equivalent to the thickness of the PCTM and an aspect ratio up to 40 was achieved (Fig. 6c). The inset shows the preserved pore entrance of ZIF-8 nanotubes. Energy-dispersive X-ray spectroscopic (EDX) mapping (Fig. 6d) and profile scanning (Fig. 6e) of the corresponding elements suggested that the structure of 1D ZIF-8 nanotubes was actually a hybrid with an amorphous PDA interface, corresponding to a poor polycrystalline structure with a relatively weak electron diffraction ring (Fig. 6b, inset). More evidence was provided by ATR-FTIR and XRD analysis. After the contra-diffusion synthesis, the resulting composite membrane, labelled as PCTM@PDA@ZIF-8, exhibited characteristic bands in the spectral region of 1411 cm^{-1} and 1307 cm^{-1} assigned to the in-plane stretching and bending of the imidazole ring, respectively (Fig. 5a, red). The absorbance at 3136 cm^{-1} and 2931 cm^{-1} was attributed to the aromatic and aliphatic C–H stretching vibrations of the 2-methylimidazole ligands.[66] This proved the incorporation of the ZIF-8 crystals into the pore arrays of PCTM templates. Meanwhile, for the isolated 1D ZIF-8 nanotubes (PDA@ZIF-8), except the characteristic peaks of ZIF-8 crystals, absorption signals of PDA, such as the broad band over 3000 cm^{-1} (catechol hydroxyl) and the clearly resolved peak at 1617 cm^{-1} (aromatic ring), were observed in the FT-IR spectrum (Fig. 5b, red), indicative of the hybridized structure of the ZIF-8 nanotubes. Besides, XRD patterns of PCTM@PDA@ZIF-8 and the isolated hybrid ZIF-8 nanotubes showed a consistency

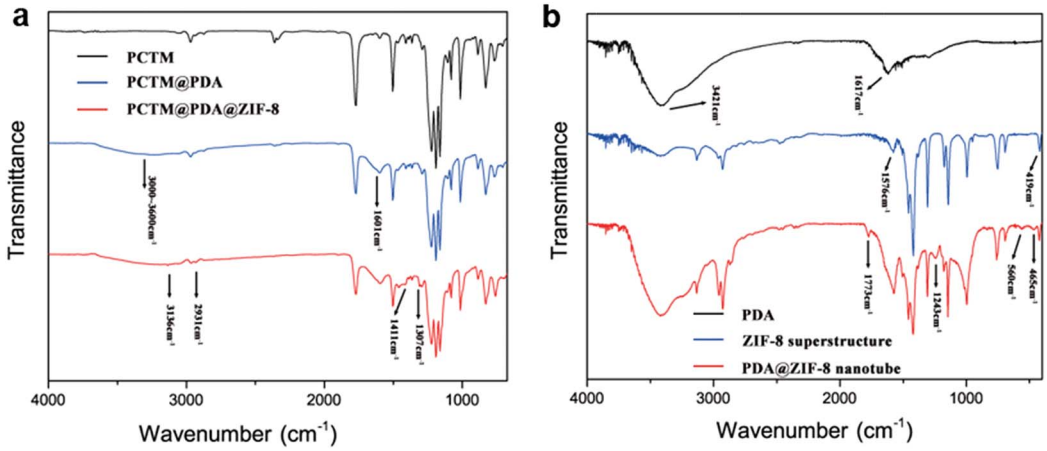

Fig. 5 (a) ATR-FTIR spectra of PCTM (black), PDA modified PCTM (blue), and the ZIF-8 immobilized counterpart (red); (b) FTIR spectra of PDA (black), 1D ZIF-8 superstructures (blue), and PDA@ZIF-8 hybrid nanotubes (red).

with native ZIF-8 crystals (Fig. 7), which also confirmed the formation of ZIF-8 crystals within the pore channels of PCTM templates.

The specific surface area and porosity of the ZIF-8 nanotubes as well as the PCTM@PDA@ZIF-8 composite membranes were evaluated by nitrogen sorption–desorption measurements at 77 K. It can be seen in Fig. 8 that both native ZIF-8 crystals and the PDA hybridized nanotubes exhibit a type-I isotherm. The BET specific surface area was estimated to be 1303 $m^2 g^{-1}$ and 1014 $m^2 g^{-1}$, respectively. The formation of the PDA hybrid structure resulted in a decrease in the BET specific surface area, which might be attributed to the shielding effect of the compact PDA shell. This also resulted in a slight decrease in pore volume from 0.71 $cm^3 g^{-1}$ of the native ZIF-8 to 0.65 $cm^3 g^{-1}$ of the hybrid ZIF-8 nanotubes. For the composite membranes, template synthesis of ZIF-8 nanotubes also introduced a large number of micropores exhibiting strong adsorption of nitrogen in the low pressure range. The BET specific surface area showed an evident increase from 13 $m^2 g^{-1}$ to 99 $m^2 g^{-1}$. Besides, preserved macropores were observed on both sides of the membranes after the contra-diffusion synthesis (Fig. S9†). The porous properties of the PCTM@PDA@ZIF-8 composite

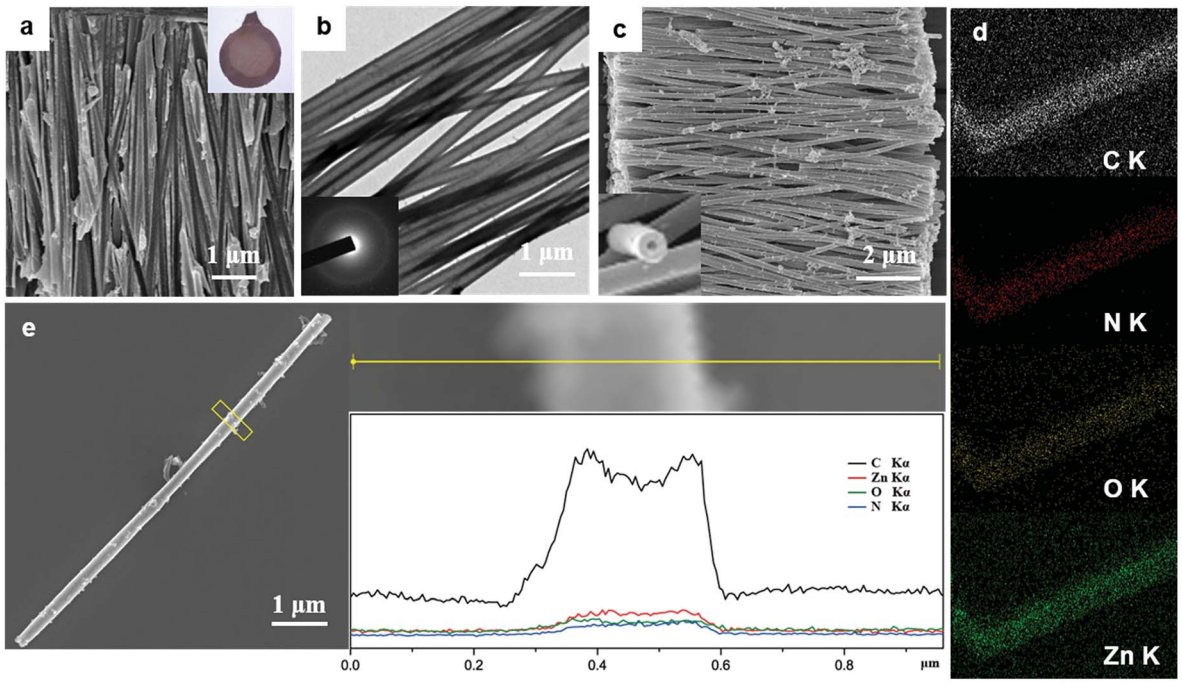

Fig. 6 (a) Section view SEM image of ZIF-8 deposited PCTM@PDA; (b) TEM and (c) SEM images of self-supported hybrid ZIF-8 nanotubes after membrane dissolution; (d) TEM EDX elemental mapping of hybrid ZIF-8 nanotubes; and (e) SEM image and the corresponding EDX spectrum profile scan of hybrid ZIF-8 nanotubes (samples pretreated by carbon spraying).

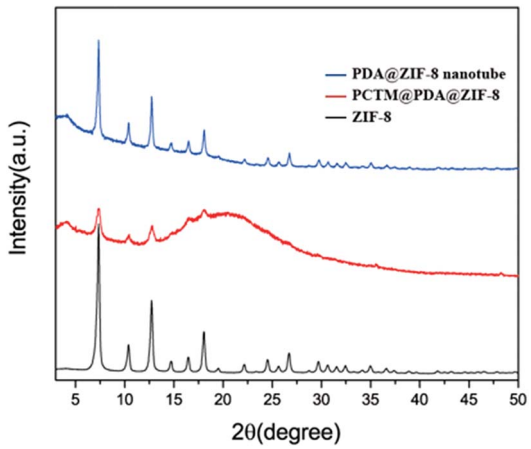

Fig. 7 XRD spectra of a native ZIF-8 crystal (black), ZIF-8 immobilized on the PDA modified PCTM (red), and PDA@ZIF-8 hybrid nanotubes (blue).

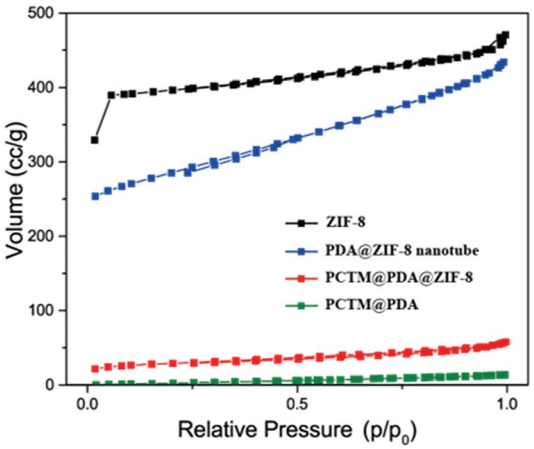

Fig. 8 N_2 sorption–desorption isotherms of the PDA modified PCTM (olive), its ZIF-8 immobilized counterpart (red), PDA@ZIF-8 hybrid nanotubes (blue), and the native ZIF-8 crystal (black) at 77 K.

membranes containing both macropores and micropores, which can balance the flux and adsorption capacity, are expected to benefit the separation applications. Thermogravimetric analysis (TGA) was used to examine the thermal stability of ZIF-8@PDA nanotubes (Fig. S10†). Only a weight loss of 5% was observed till 500 °C, corresponding to the removal of guest and unreacted molecules. The thermal stability of ZIF-8@PDA nanotubes was further evaluated by heating at 250 °C under N_2 for 24 hours. After the heating treatment, the nanotubes presented no distinct change in crystal structure and morphology (Fig. S11†), which confirmed the thermal stability of the nanotubes.

As demonstrated above, the introduction of PDA to the inner surfaces of the pore arrays of PCTM promoted the template synthesis of 1D ZIF-8 superstructures. Here, the PDA served as a coordination platform to accommodate zinc ions, which facilitated the heterogeneous nucleation and growth of ZIF-8 crystals, as well as an interface-strengthening agent to improve the structural stability of the resulting 1D superstructures. First, due to the existence of abundant catechol and amine species, PDA can effectively coordinate with transition metal ions, including Zn(II), *via* the formation of metal–catechol and/or metal–nitrogen–donor complexes.[67,68] Upon contact with the imidazole ligands, the Zn(II) anchored sites acted as nucleation centers to induce the confined growth of ZIF-8 crystals on the PDA surface, preventing the formation of discrete ZIF-8 crystals in the solution to block the diffusion path of the imidazole ligands. Therefore, hollow ZIF-8 nanotubes with uniform channels spanning across the channels of the membrane were obtained. On the other hand, it has been reported that the metal–catechol coordination complexes may exhibit near-covalent stiffness and strength.[66] This would stabilize the intergrown ZIF-8 crystals, resulting in well-defined 1D hybrid ZIF-8 nanotubes after the dissolution of the PCTM templates.

The versatility of the PDA mediated template synthesis strategy was examined for preparing 1D superstructures for other kinds of MOFs. Following the established procedure, contra-diffusion synthesis of ZIF-67, ZIF-12, and HKUST-1 was performed. Due to the structural and compositional similarity with ZIF-8, ZIF-67 exhibited a confined growth behavior along the pore walls of the PCTM template (Fig. 9a). Self-supported 1D ZIF-67 nanotubes with uniform channels and a length equivalent to the membrane thickness were obtained (Fig. 9b). But for ZIF-12, relatively large-sized particles were observed in the section view SEM image (Fig. 9c), and hollow 1D ZIF-12 superstructures with a reduced aspect ratio were finally obtained (Fig. 9d). ZIF-12 is composed of cobalt nodes coordinated with benzimidazole (bIM) ligands. Since PDA could also provide strong binding to the cobalt ions, the limited length of the ZIF-12 superstructures might be attributed to the diffusion hindrance of the bIM ligands in the PDA modified pore channels. Unlike the mIM ligands, bIM is a heterocyclic aromatic compound with the fusion of benzene and imidazole units. Thus, the diffusion of bIM ligands would be hindered to some extent due to the strong interactions with the PDA layer, such as π–π stacking and hydrogen bonding, thereby resulting in a limited diffusion path and uncontinuous growth of ZIF-12 crystals in the pore channels. Interestingly, with the introduction of PDA, HKUST-1 showed a different growth behavior during the contra-diffusion synthesis, as compared to the situation within native PCTM templates. HKUST-1 particles with a decreased size (less than 260 nm) were formed in the pore channels (Fig. 9e). And the confined growth of HKUST-1 crystals on the PDA surface generated 1D hollow superstructures with a length >2 μm instead of short HKUST-1 nanorods (Fig. 9f). This demonstrated the benefits of PDA for the anchoring of MOFs on an inert surface. Nonetheless, due to the relatively large crystal size of HKUST-1 as well as the diffusion limits of the aromatic BTC ligands, it remains challenging to prepare longer 1D hollow HKUST-1 nanotubes with ideal channels. The XRD and FTIR results of the corresponding MOFs are listed from Fig. S12 to S17,† confirming the formation of MOF crystals in the pores of the template as well as the nanotubes.

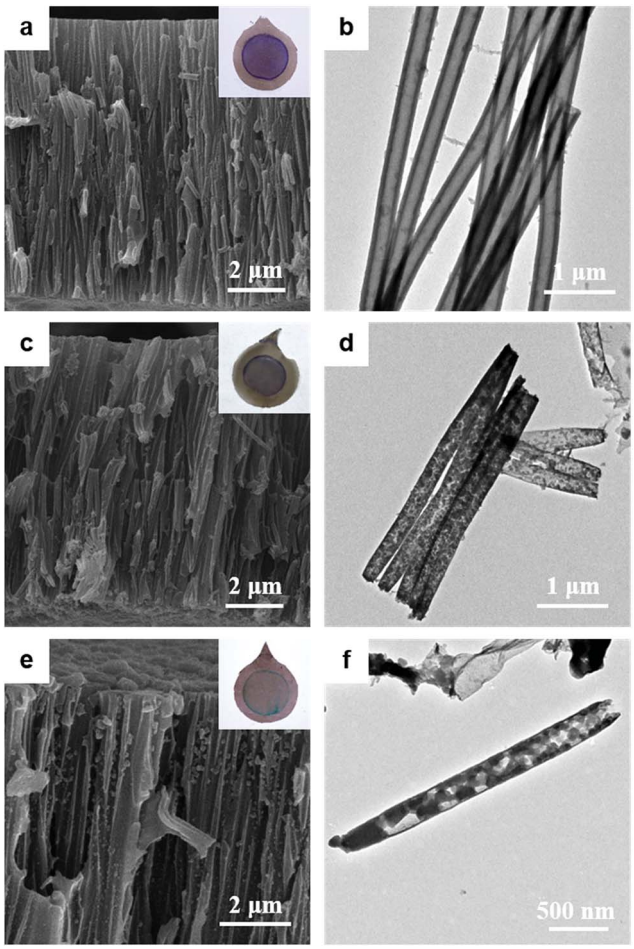

Fig. 9 Section view SEM images of (a) ZIF-67, (c) ZIF-12 and (e) HKUST-1 grown on the PDA modified PCTM. The insets are the digital photos of the corresponding composite membranes; TEM images of 1D hybrid (b) ZIF-67, (d) ZIF-12 and (f) HKUST-1 nanotubes after membrane dissolution.

Subsequently, we examined the potential application of the composite membrane for separation of methylene blue, a typical organic contaminant in wastewater. Taking advantage of the ZIF-8 functionalized composite membrane, effective separation of the organic dye was achieved using a simple filtration mode. A digital photo of the ZIF-8 composite membrane is shown in Fig. 6a (inset) with a functionalized area of 1.2 cm^2. Under a flow rate of 3 mL min^{-1}, the methylene blue in the solution was readily separated. The UV-vis spectra of the original methylene blue solution and the filtrates across the composite membrane are shown in Fig. 10. With the confined growth of ZIF-8 in the pore channels, the functionalized composite membrane showed a removal ratio of 92% for methylene blue. The composite membrane can be regenerated by immersion in methanol for one hour and can be reused at least three times without a distinct loss of removal ratio (Fig. S18†) and change in morphology (Fig. S19 and 20†). Such performance is fairly good for single-stage filtration in consideration of the continuous multi-stage feature of the membrane separation process, suggesting the promising application of the

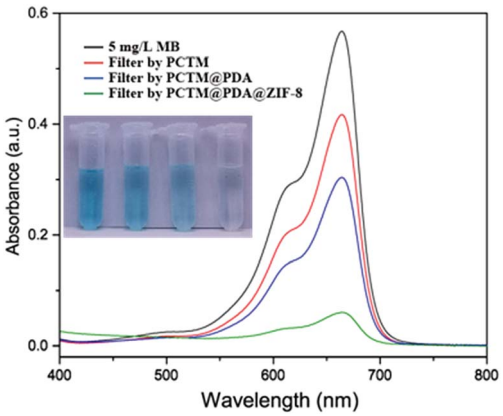

Fig. 10 UV-vis spectra of methylene blue solution (5 mg L^{-1}) and its counterparts after filtration through PCTM, PCTM@PDA and PCTM@PDA@ZIF-8 under a flow rate of 3 mL min^{-1}, respectively. The inset shows a digital photo of the corresponding methylene blue solutions.

MOF-functionalized PCTM for separation of chemical and biological molecules. In contrast, due to the weak interactions between polycarbonate and ZIF-8, the ZIF-8 composite membrane without the PDA deposition procedure showed either loss of ZIF-8 from membranes or block on membranes. The difference depends on the length of contra-diffusion synthesis time and shows an indefinite boundary around 30 minutes. All the unblocked samples showed a removal ratio no more than 38%, highlighting the significant interface-strengthening of mussel-inspired PDA chemistry in the adhesive and support for the fabrication of composite membrane and robust 1D MOFs.

Conclusion

In summary, this study presents a facile and adaptable contra-diffusion synthesis of 1D MOF superstructures within the pore arrays of polycarbonate track-etched membranes (PCTMs) by tuning the surface chemistry. In a native PCTM template, the nucleation and growth of ZIF-8 could be promoted according to a catalytic transesterification mechanism to activate the specific imidazole ligands. Surface modification of the pore channels by the bio-inspired polydopamine (PDA) chemistry provided better controllability to regulate the template synthesis of MOFs. PDA served as anchor bars of metal ions, facilitating the confined growth of MOF crystals with reduced size to form well-defined nanotubes with uniform channels, and also as an interface-strengthening agent for the fabrication of robust 1D MOF superstructures after template removal. 1D hybrid ZIF-8 nanotubes spanning across the entire thickness of the template (10 μm) were obtained with an aspect ratio reaching up to 40. The versatility of the PDA mediated template synthesis strategy has been demonstrated in preparing 1D superstructures for other MOFs such as ZIF-67, ZIF-12, and HKUST-1 with different morphologies. The as-synthesized ZIF-8 integrated PCTM was proved to be able to effectively separate the organic dye in a filtration system. To conclude, this study provides new insight

into the surface chemistry directed growth behavior of MOFs within confined channels of polymeric templates. Furthermore, the PDA mediated synthetic strategy is believed to bring about vast opportunities for template synthesis of more MOF superstructures for diverse applications.

Conflicts of interest

There are no conflicts to declare.

Acknowledgements

The study was supported by the Changjiang Scholars and Innovative Research Team in University (IRT13026), the National Science Fund for Distinguished Young Scholars (51425403), the National Natural Science Foundation of China under Projects 51673109, 51473087 and U1430234.

References

1 H. Furukawa, K. E. Cordova, M. O'Keeffe and O. M. Yaghi, *Science*, 2013, **341**, 123044.
2 H. C. Zhou, J. R. Long and O. M. Yaghi, *Chem. Rev.*, 2012, **112**, 673–674.
3 B. Li, M. Chrzanowski, Y. Zhang and S. Ma, *Coord. Chem. Rev.*, 2016, **307**, 106–129.
4 W. Y. Gao, M. Chrzanowski and S. Ma, *Chem. Soc. Rev.*, 2014, **43**, 5841–5866.
5 H. C. Zhou and S. Kitagawa, *Chem. Soc. Rev.*, 2014, **43**, 5415–5418.
6 B. Li, H. M. Wen, Y. Cui, W. Zhou, G. Qian and B. Chen, *Adv. Mater.*, 2016, **28**, 8819–8860.
7 H. Li, K. Wang, Y. Sun, C. T. Lollar, J. Li and H.-C. Zhou, *Mater. Today*, 2018, **21**, 108–121.
8 Y. He, B. Li, M. O'Keeffe and B. Chen, *Chem. Soc. Rev.*, 2014, **43**, 5618–5656.
9 S. Ma and H.-C. Zhou, *Chem. Commun.*, 2010, **46**, 44–53.
10 H. Yang, F. Guo, P. Lama, W.-Y. Gao, H. Wu, L. Barbour, W. Zhou, J. Zhang, B. Aguila and S. Ma, *ACS Cent. Sci.*, 2018, **4**, 1194–1200.
11 A. Corma, H. García and F. X. Llabrés i Xamena, *Chem. Rev.*, 2010, **110**, 4606–4655.
12 Z. Niu, W. D. C. B. Gunatilleke, Q. Sun, P. C. Lan, J. Perman, J.-G. Ma, Y. Cheng, B. Aguila and S. Ma, *Chem*, 2018, **4**, DOI: 10.1016/j.chempr.2018.08.018.
13 Y. B. Huang, J. Liang, X. S. Wang and R. Cao, *Chem. Soc. Rev.*, 2017, **46**, 126–157.
14 M. J. Kalmutzki, C. S. Diercks and O. M. Yaghi, *Adv. Mater.*, 2018, 1704304, DOI: 10.1002/adma.201704304.
15 L. Zhu, D. Sheng, C. Xu, X. Dai, M. A. Silver, J. Li, P. Li, Y. Wang, Y. Wang, L. Chen, C. Xiao, J. Chen, R. Zhou, C. Zhang, O. K. Farha, Z. Chai, T. E. Albrecht-Schmitt and S. Wang, *J. Am. Chem. Soc.*, 2017, **139**, 14873–14876.
16 J. Li, X. Wang, G. Zhao, C. Chen, Z. Chai, A. Alsaedi, T. Hayat and X. Wang, *Chem. Soc. Rev.*, 2018, **47**, 2322–2356.
17 S. Qiu, M. Xue and G. Zhu, *Chem. Soc. Rev.*, 2014, **43**, 6116–6140.
18 M. X. Wu and Y. W. Yang, *Adv. Mater.*, 2017, **29**, 1606134.
19 Y. Feng, X. Y. Yu and U. Paik, *Chem. Commun.*, 2016, **52**, 6269–6272.
20 Y. Cui, B. Li, H. He, W. Zhou, B. Chen and G. Qian, *Acc. Chem. Res.*, 2016, **49**, 483–493.
21 X. Lian and B. Yan, *RSC Adv.*, 2016, **6**, 11570–11576.
22 S. Norbert and B. Shyam, *Chem. Rev.*, 2011, **112**, 933–969.
23 A. Carne-Sanchez, I. Imaz, K. C. Stylianou and D. Maspoch, *Chem.–Eur. J.*, 2014, **20**, 5192–5201.
24 E. A. Flügel, A. Ranft, F. Haase and B. V. Lotsch, *J. Mater. Chem.*, 2012, **22**, 10119–10133.
25 J. Deng, D. Deng and X. Bao, *Adv. Mater.*, 2017, **29**, 1606967.
26 M. Pang, A. J. Cairns, Y. Liu, Y. Belmabkhout, H. C. Zeng and M. Eddaoudi, *J. Am. Chem. Soc.*, 2012, **134**, 13176–13179.
27 P. Pachfule, B. K. Balan, S. Kurungot and R. Banerjee, *Chem. Commun.*, 2012, **48**, 2009–2011.
28 M. Drobek, J. H. Kim, M. Bechelany, C. Vallicari, A. Julbe and S. S. Kim, *ACS Appl. Mater. Interfaces*, 2016, **8**, 8323–8328.
29 M. Jahan, Q. Bao, J. X. Yang and K. P. Loh, *J. Am. Chem. Soc.*, 2010, **132**, 14487.
30 M. Jian, H. Wang, R. Liu, J. Qu, H. Wang and X. Zhang, *Environ. Sci.: Nano*, 2016, **3**, 1186–1194.
31 W. W. Zhan, Q. Kuang, J. Z. Zhou, X. J. Kong, Z. X. Xie and L. S. Zheng, *J. Am. Chem. Soc.*, 2013, **135**, 1926–1933.
32 W. Zhang, Z. Y. Wu, H. L. Jiang and S. H. Yu, *J. Am. Chem. Soc.*, 2014, **136**, 14385–14388.
33 T. Tsuruoka, S. Furukawa, Y. Takashima, K. Yoshida, S. Isoda and S. Kitagawa, *Angew. Chem., Int. Ed. Engl.*, 2009, **48**, 4739–4743.
34 J. Puigmarti-Luis, M. Rubio-Martinez, U. Hartfelder, I. Imaz, D. Maspoch and P. S. Dittrich, *J. Am. Chem. Soc.*, 2011, **133**, 4216–4219.
35 P. Pachfule, S. Kandmabeth, A. Mallick and R. Banerjee, *Chem. Commun.*, 2015, **51**, 11717–11720.
36 M. Gualino, N. Roques, S. Brandès, L. Arurault and J.-P. Sutter, *Cryst. Growth Des.*, 2015, **15**, 3552–3555.
37 W. T. Koo, J. S. Jang, S. J. Choi, H. J. Cho and I. D. Kim, *ACS Appl. Mater. Interfaces*, 2017, **9**, 18069–18077.
38 L. V. Meyer, J. Vogt, F. A. Brede, H. Schäfer, M. Steinhart and K. Müller-Buschbaum, *CrystEngComm*, 2013, **15**, 9382–9386.
39 N. Liu, Y. Yao, J. J. Cha, M. T. McDowell, Y. Han and Y. Cui, *Nano Res.*, 2011, **5**, 109–116.
40 M. Maksoud, N. Roques, S. Brandès, L. Arurault and J.-P. Sutter, *J. Mater. Chem. A*, 2013, **1**, 3688–3693.
41 M. He, J. Yao, Z.-X. Low, D. Yu, Y. Feng and H. Wang, *RSC Adv.*, 2014, **4**, 7634–7639.
42 H. Lee, S. M. Dellatore, W. M. Miller and P. B. Messersmith, *Science*, 2007, **318**, 426–430.
43 Z. Zeng, M. Wen, G. Ye, X. Huo, F. Wu, Z. Wang, J. Yan, K. Matyjaszewski, Y. Lu and J. Chen, *Chem. Mater.*, 2017, **29**, 10212–10219.
44 Y. Song, G. Ye, F. Wu, Z. Wang, S. Liu, M. Kopeć, Z. Wang, J. Chen, J. Wang and K. Matyjaszewski, *Chem. Mater.*, 2016, **28**, 5013–5021.
45 M. Liu, G. Zeng, K. Wang, Q. Wan, L. Tao, X. Zhang and Y. Wei, *Nanoscale*, 2016, **8**, 16819–16840.
46 Y. Liu, K. Ai and L. Lu, *Chem. Rev.*, 2014, **114**, 5057–5115.

47 C. T. Chen, F. J. Martin-Martinez, G. S. Jung and M. J. Buehler, *Chem. Sci.*, 2017, **8**, 1631–1641.
48 J. Zhou, P. Wang, C. Wang, Y. T. Goh, Z. Fang, P. B. Messersmith and H. Duan, *ACS Nano*, 2015, **9**, 6951–6960.
49 M. Zhao, C. Deng and X. Zhang, *Chem. Commun.*, 2014, **50**, 6228–6231.
50 A. Huang, Q. Liu, N. Wang, Y. Zhu and J. Caro, *J. Am. Chem. Soc.*, 2014, **136**, 14686–14689.
51 J. Yao, D. Dong, D. Li, L. He, G. Xu and H. Wang, *Chem. Commun.*, 2011, **47**, 2559–2561.
52 M. He, J. Yao, L. Li, Z. Zhong, F. Chen and H. Wang, *Microporous Mesoporous Mater.*, 2013, **179**, 10–16.
53 K. Huang, Q. Li, G. Liu, J. Shen, K. Guan and W. Jin, *ACS Appl. Mater. Interfaces*, 2015, **7**, 16157–16160.
54 R. L. Fleischer and P. B. Price, *Geochim. Cosmochim. Acta*, 1964, **28**, 1705–1714.
55 P. Apel, *Radiat. Meas.*, 2001, **34**, 559–566.
56 S. Gryglewicz, F. A. Oko and G. Gryglewicz, *Ind. Eng. Chem. Res.*, 2003, **42**, 5007–5010.
57 C. Chizallet, S. Lazare, D. Bazerbachi, F. Bonnier, V. Lecocq, E. Soyer, A. A. Quoineaud and N. Bats, *J. Am. Chem. Soc.*, 2010, **132**, 12365–12377.
58 R. Demir-Cakan, P. Makowski, M. Antonietti, F. Goettmann and M.-M. Titirici, *Catal. Today*, 2010, **150**, 115–118.
59 H. Yuan, Y. Lu, Z. Wang, Z. Ren, Y. Wang, S. Zhang, X. Zhang and J. Chen, *Chem. Commun.*, 2016, **52**, 1808–1811.
60 H. Yuan, J. Liu, Y. Lu, Z. Wang, G. Wei, T. Wu, G. Ye, J. Chen, S. Zhang and X. Zhang, *Anal. Chem.*, 2017, **89**, 1045–1048.
61 D. J. Tranchemontagne, J. R. Hunt and O. M. Yaghi, *Tetrahedron*, 2008, **64**, 8553–8557.
62 R. Parker, in *Solid State Physics*, Elsevier, 1970, vol. 25, pp. 151–299.
63 M. C. McCarthy, V. Varela-Guerrero, G. V. Barnett and H. K. Jeong, *Langmuir*, 2010, **26**, 14636–14641.
64 Z. Meimei, L. Jian, Z. Meng, W. Hui, L. Yue, W. Yi-Nan, L. Fengting and L. Guangtao, *Chem. Commun.*, 2015, **51**, 2706–2709.
65 F. Yu, S. Chen, Y. Chen, H. Li, L. Yang, Y. Chen and Y. Yin, *J. Mol. Struct.*, 2010, **982**, 152–161.
66 B. Hachuła, M. Nowak and J. Kusz, *J. Chem. Crystallogr.*, 2010, **40**, 201–206.
67 Z. Xu, *Sci. Rep.*, 2013, **3**, 2914.
68 H. Wu, J. M. Ang, J. Kong, C. Zhao, Y. Du and X. Lu, *RSC Adv.*, 2016, **6**, 103390–103398.